Electronic Supplementary Information

Valence Holes Observed in Nanodiamonds Dispersed in Water

Tristan Petit*[1], Mika Pflüger*[2], Daniel Tolksdorf[2], Jie Xiao[1], and Emad F. Aziz[1,2,3]

[1]Institute of Methods for Materials Development, Helmholtz-Zentrum Berlin, Albert-Einstein-Str. 15, 12489 Berlin, Germany
[2]Freie Universität Berlin, FB Physik, Arnimallee 14, 14195 Berlin, Germany
[3]Institute of Molecular Science, Myodaiji, Okazaki, 444-8585, Japan

Corresponding Author: Tristan Petit, E-mail tristan.petit@helmholtz-berlin.de

*These authors contributed equally to the work.

1 Experimental Methods

Water-based dispersions of detonation NDs produced by Plasmachem (Single-Digit Nanodiamonds, 5 %wt) were characterized. Further dilution was performed with deionized water (0.05 µS/cm). XAS and XES measurements were carried out with the LiXEdrom end-station at the U41-PGM undulator beamline of the BESSY II synchrotron facility of the Helmholtz-Zentrum Berlin. More details about this experimental setup are available in [Lan10]. The beamline resolution for the carbon and oxygen K edges is approximately 0.1 eV. The XA spectra were recorded in the TFY mode using a $5\,\mathrm{mm}^2 \times 5\,\mathrm{mm}^2$ GaAsP photodiode (Hamamatsu GaAsP G1127-4) at a 45° angle with respect to the beamline. The XE measurements were performed using a MCP - fluorescent screen - CCD detector (Gamma Data) setup in combination with a grating (1200 lines/mm, grating radius of 5m for C K edge and 7.5m for O K edge) in Rowland-geometry with the liquid microjet as the photon emitting source in a slit-less configuration. The ND dispersion flows in the high-pressure liquid microjet using glass nozzles of 20 µm to 22 µm diameter with a flow rate of 0.6 ml/ min to 0.8 ml/ min after filtration through a 2 µm pore size filter. The exposure time of NDs to X-rays resulting from the high speed of the flow is estimated to be in the order of 1 µs to 2 µs. In addition, the efficient cooling of NDs by surrounding water molecules avoids sample damage in the microjet. Measurements were performed at a pressure of approximately $10 \cdot 10^{-5}$ mbar with the microjet and at $10 \cdot 10^{-7}$ mbar for dried samples. XAS spectra were normalized to the photon flux after background signals from carbon impurities and water contribution were taken into account (see next section). Energy calibration for XES was done using the elastic scattering feature measured at different excitation energies. For XES microjet measurements at carbon K edge, the contribution from second order diffraction of oxygen K edge signal was close to the carbon first order signal. Its signal is thus subtracted, as detailed in the last section.

2 Background correction procedure for X-ray absorption measurements

For absorption measurements, analysis of the raw total fluorescence yield spectra is complicated by two problems: background signals and variations in x-ray photon flux. Background signals are produced mainly by the fluorescence of contaminations (for film samples) or solvent (for liquid samples), either by absorption of x-rays at the measurement energy (e.g. off-resonant carbon K-edge absorption at oxygen K-edge energies) or by absorption of higher harmonics, which have intensities up to 10 % at the used beamline (e.g. off-resonant oxygen K-edge absorption of x-rays with twice the energy of carbon K-edge measurements). Nevertheless, higher harmonics of used excitation energies are far above relevant absorption edges, such that the largest part of the background is not energy dependent. The x-ray photon flux was measured with a GaAs photodiode inserted directly into the x-ray beam before and after sample measurements. It is very stable over time for the normal "top-up" mode of operation in BESSY-II, with variations smaller than $\approx 1\,\%$. Unfortunately, the energy dependence of the x-ray photon flux is much more pronounced, especially at the carbon edge (see figure S1) and has to be compensated in order to obtain reliable results.

Putting this together, an energy-dependent measured XAS signal $m(E)$ is considered to be composed of a sample signal $x(E)$ plus an energy-dependent signal stemming from impurities or solvent $s(E)$, both modulated by the photon flux of the first harmonic $p(E)$. Additionally, there is a constant background B from the non energy-dependent off-resonant absorption of higher

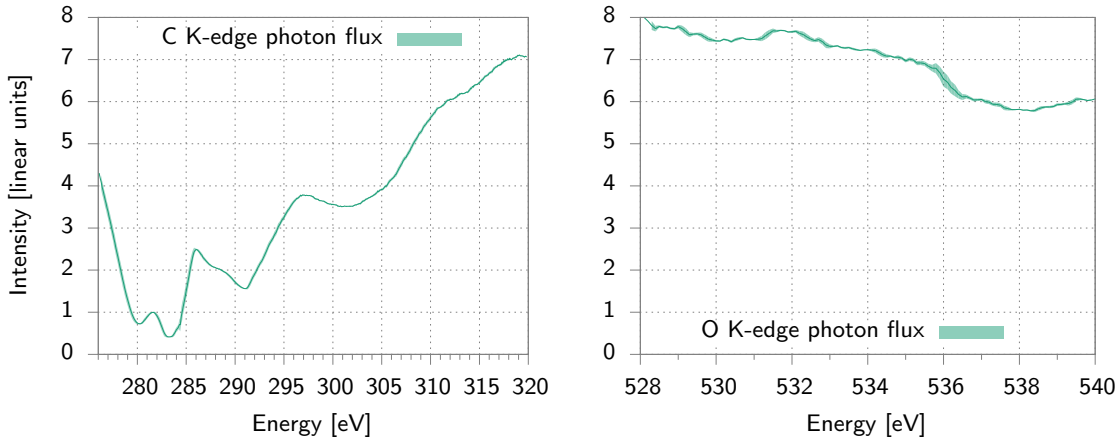

Figure S1: Intensity of the photon flux of the U41PGM beamline measured by a GaAs photodiode. The shown uncertainty is the 1σ standard deviation of a region $\pm 0.2\,\mathrm{eV}$ around each measurement point. On the left are energies around the carbon K-edge, on the right around the oxygen K-edge. The intensities are not comparable between the edges. As can be seen, the changes in photon flux over the relevant energy range are much more pronounced at the carbon K-edge than on the oxygen K-edge.

harmonics:

$$m(E) = p(E)\,(x(E) + s(E)) + B\,. \tag{1}$$

Depending on the type of measurement, some parts can be neglected or have to be taken into account, thus we will discuss the cases seperately.

Statistical errors on the spectra are estimated as the standard deviation from multiple measurements and correlated gaussian error propagation is used throughout the data analysis. The energy reproduction error of the beamline (the possible difference in central beam energy from two grating repositions targetting the same energy) was found to be $\approx 0.2\,\mathrm{eV}$ by observing the position of the very sharp crystalline diamond K-edge excitonic peak of multiple measurements. For each data point of the photon flux, the uncertainty was estimated as the standard deviation of the measurements in a $\pm 0.2\,\mathrm{eV}$ window, incorporating the energy reproduction error of the beamline into the data analysis. For all fitted values, the uncertainty of the fitted parameters was estimated from the goodness of the fit and the results covariance matrix as correlated errors.

2.1 Solid Film Measurements

For solid films, the impurities are small compared to the carbon content, such that first-harmonic measurements are dominated by the sample signal, i.e. $s(E) \approx 0$. Our measurement equation simplifies to

$$m(E) = p(E)\,x(E) + B\,. \tag{2}$$

To extract $x(E)$ from the measurement, the photon flux $p(E)$ was measured using a GaAs photodiode directly exposed to the incident beam. The constant background B can be neglected in oxygen K edge measurements due to the high photon flux at the oxygen K edge, which yields the sample signal as $x(E) \approx m(E)/p(E)$.

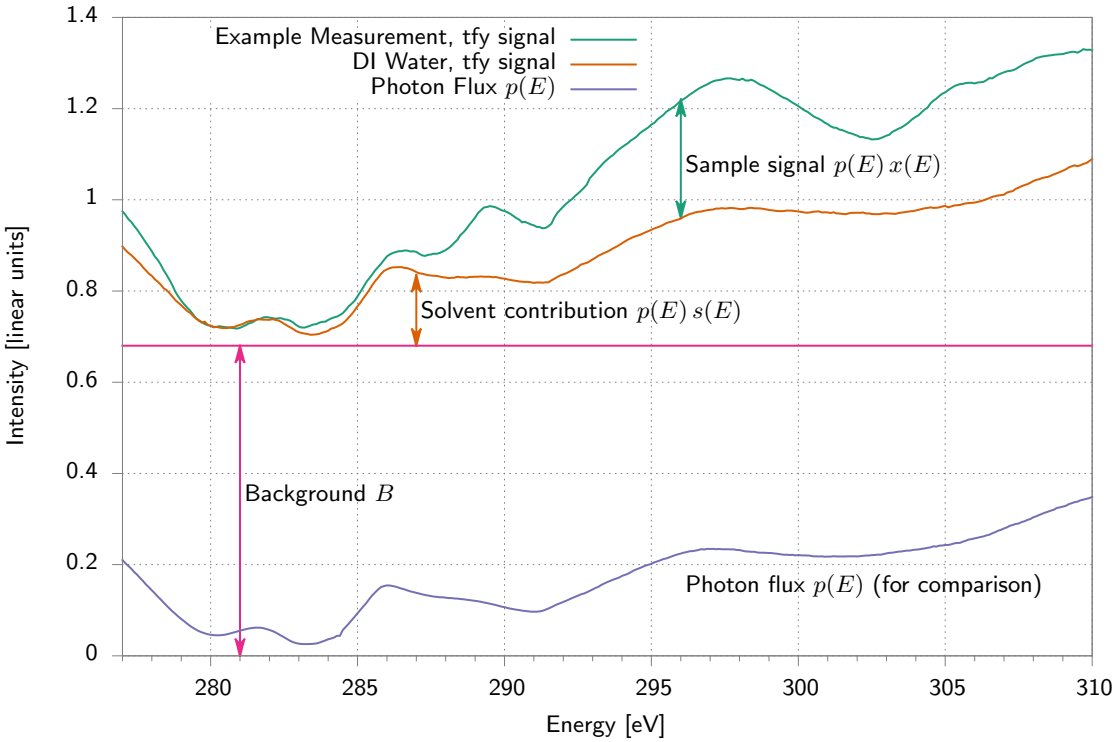

Figure S2: Exemplary XAS tfy measurement with relevant contributions. The measurement is composed of a large constant background B, an energy-dependent contribution from the solvent $s(E)$, which is modulated by the photon flux $p(E)$ and finally the sample signal $x(E)$, which is also modulated by the photon flux $p(E)$. The photon flux is shown for comparison. As the example measurement, a liquid jet measurement of nanodiamonds in suspension is used. All uncertainty indications are omitted for clarity.

At the carbon K edge the photon flux is unfortunately orders of magnitude lower and therefore B is very high, actually many times higher than $p(E)\,x(E)$, such that it can not be neglected. To estimate B, it was assumed that in the energy region well before the carbon K edge, the signal $x(E)$ is zero, i.e.

$$m(E \text{ of pre-edge}) \approx B \quad \text{such that} \tag{3}$$

$$\sum_{E \text{ of pre-edge}} \left| \frac{m(E) - B}{p(E)} \right|^2 \approx \sum_{E \text{ of pre-edge}} |x(E)|^2 \tag{4}$$

was minimized by fitting B using linear least squares. The approximate sample signal was then acquired as $x(E) = (m(E) - B)/p(E)$.

2.2 Liquid Measurements

Again, for liquid measurements the oxygen K edge is comparatively simple to analyze. With water as the solvent, the oxygen signal is so strong that background effects can be neglected and the approximate sample signal can be acquired as $x(E) = m(E)/p(E)$ as in the solid film oxygen K edge measurements.

On the other hand, carbon K edge measurements of colloidal suspensions are dominated by background signals, as the oxygen atom molar concentration is over 50 times higher than the carbon atom molar concentration at 1 Wt% ND concentration. Thus, background effects occur in both first and higher harmonic absorption, such that $s(E) \neq 0$ and with $B >> p(E)\,x(E)$. The constant offset B is especially high since the contaminations in the beamline reduce the flux at carbon energies, but without significantly reducing higher harmonics; therefore, the signal from higher harmonics is significantly enhanced. So we have to assume the most general model for our measurement,

$$m(E) = p(E)\,(x(E) + s(E)) + B\,. \tag{5}$$

In order to extract $x(E)$ from the measurement, we measured the pure solvent signal (i.e. pure water) $m_s(E)$, which is modeled as

$$m_s(E) = (p(E)\,s(E) + B)T + A\,, \tag{6}$$

where T is a factor to account for different alignment of the beam onto the microjet, which will scale the whole signal, and A accounts for a stronger or weaker background (which in general does not scale equally to the rest of the signal). T and A are estimated again using the fact that at certain energies pre-edge $x(E \text{ of pre-edge}) \approx 0$, thus

$$\sum_{E \text{ of pre-edge}} |m(E) - (m_s(E) - A)/T|^2 \approx \sum_{E \text{ of pre-edge}} |p(E)\,x(E)|^2 \tag{7}$$

was minimized using the method of linear least squares as implemented in the numpy package *polyfit* function. Combining this result with the measurement of $p(E)$ as before, we get:

$$\frac{m(E) - (m_s(E) - A)/T}{p(E)} \approx \frac{p(E)\,(x(E) + \cancel{s(E)}) + \cancel{B} - \cancel{p(E)\,s(E)} - \cancel{B}}{p(E)} = x(E)\,, \tag{8}$$

finally giving us our sample signal $x(E)$.

2.3 Piecewise Measurements

In order to minimize sample damage in solid film measurements and to minimize signal drift in liquid jet measurements, it is sometimes useful to measure smaller energy ranges to have shorter measurement times. Measurement ranges were chosen to overlap for at least 10 measurement points and the pieces were then connected by estimating a correction factor as the mean of the ratio of the common points, i.e. for two measurements $m_1(E)$ and $m_2(E)$ it was assumed

$$m_1(E \text{ common}) = m_2(E \text{ common})\,T \tag{9}$$

$$\Rightarrow T \approx \overline{\left(\frac{m_1(E \text{ common})}{m_2(E \text{ common})}\right)} \tag{10}$$

$$\Rightarrow m_{\text{combined}}(E) = m_1(E) \text{ or } m_2(E)\,T \quad \text{depending on energy,} \tag{11}$$

with $m_{\text{combined}}(E)$ the resulting combined measurement.

2.4 Averaging Several Measurements

For some measurements, it was necessary to reduce noise levels by averaging several individual measurements. Unfortunately, for each measurement the setup was aligned slightly differently (most notably for microjet measurements the microjet would be a bit thicker or oriented slightly differently), leading to a different signal strength and background, so in the general form

$$m(E) = C\,(p(E)\,(x(E) + s(E)) + B)\,. \tag{12}$$

C and B would be different between two measurements. In order to properly average several measurements, the measurements have to be normalized for common parameters C and B first, which is done by fitting them to a provisional average using linear least squares. After this correction, the mean of the measurements is taken and the standard deviation of the measurements at each energy point is used as the uncertainty, which is propagated through the rest of the analysis as described above.

3 Background correction procedure for X-ray emission measurements

The detector position was optimized to second order signals from the oxygen K edge for the measurements on water and aqueous samples in the microjet, to first order signals for all carbon K edge measurements. In the case of carbon K edge emission from nanodiamonds in water, second order contributions from the oxygen K edge are also detected, due to the close proximity of the carbon K edge ($\approx 280\,\mathrm{eV}$) to half the energy of the oxygen edge ($\approx 530/2\,\mathrm{eV} = 265\,\mathrm{eV}$). The oxygen contributions result from excitation of water molecules by higher beamline harmonics (mainly second harmonics at $\approx 640\,\mathrm{eV}$). The uncorrected signal can be seen in figure S3a. This oxygen contribution was measured on pure water (fig. S3b) and subtracted from the carbon K edge signal (fig. S3c). The oxygen peak position was also used together with the energies of elastic peaks of different excitation energies for energy calibration of the carbon K edge detector position.

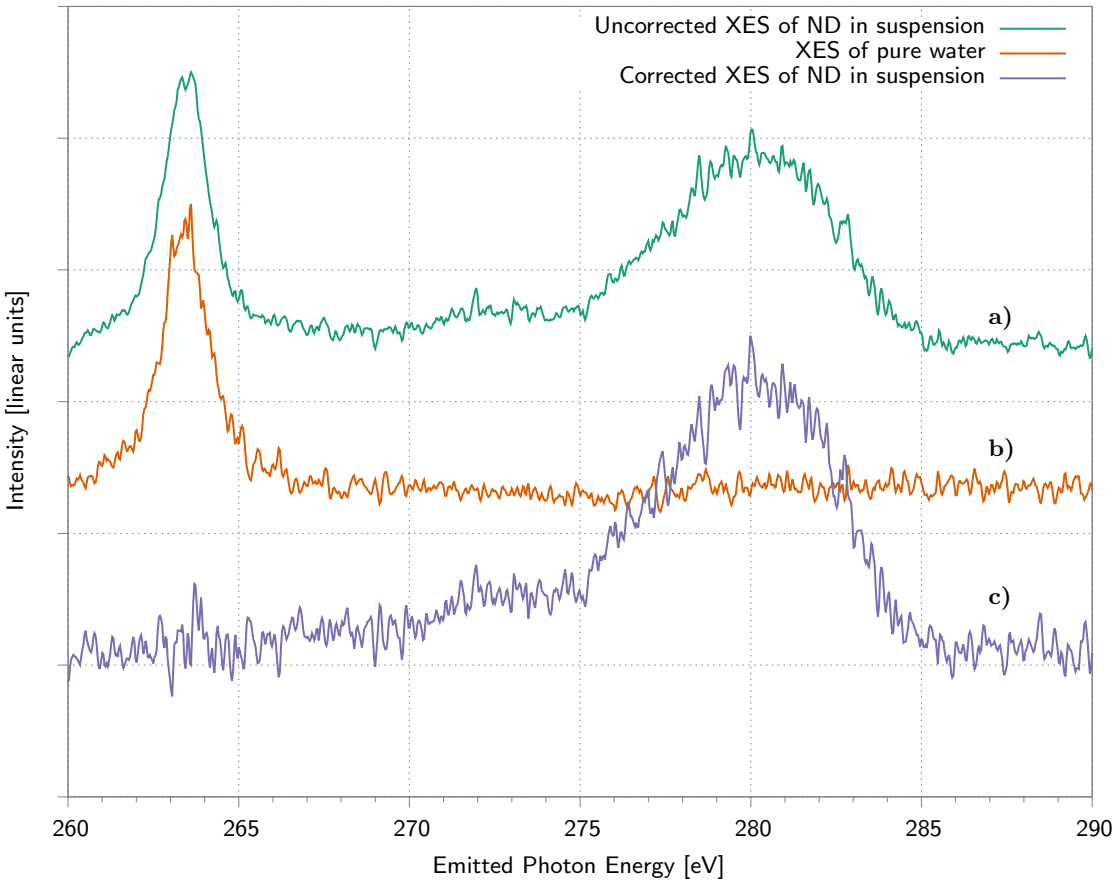

Figure S3: a) Raw x-ray emission spectrum of nanodiamonds in suspension, excited at 320 eV. On the left is the second-order contribution of water oxygen, on the right the first-order of nanodiamond carbon. b) X-ray emission of pure water, with only the oxygen contribution, also excited at 320 eV. c) Corrected XES of nanodiamonds in suspension, calculated as $a - b$.

References

[Lan10] K. M. Lange, R. Könnecke, S. Ghadimi, R. Golnak, M. A. Soldatov, K. F. Hodeck, A. Soldatov, and E. F. Aziz. High resolution X-ray emission spectroscopy of water and aqueous ions using the micro-jet technique. *Chemical Physics*, 377:1–5, 2010. doi:10.1016/j.chemphys.2010.08.023.